State estimation of low voltage distribution network with integrated customer-owned PV and storage unit

Motaz Ayiad
Hugo Martins

EFACEC
Porto, Portugal

Onyema Nduka
Bikash Pal

Control and Power Research Group
Imperial College London, United Kingdom

***Abstract*—The growing integration of rooftop photovoltaics (PVs) and energy storage units (ESUs) in customer households has resulted in changes in the customer load profiles. This is likely to influence the accuracy of state estimation (SE) carried out based on previously assumed load profiles. In this paper, a statistical model for modern low voltage (LV) customers was developed using Gaussian mixture model (GMM). The resulting model was subsequently applied to SE using weighted least squares (WLS) algorithm. LV network with high penetration of customer-owned PV and ESUs have been simulated. Different scenarios which include load profiles: with PVs integrated but without ESUs, ESUs alone, and with hybrid systems (combination of PVs and ESUs) have been considered. The results are presented and discussed.**

***Index Terms*—Distribution networks, energy storage units, Gaussian mixture model, photovoltaics, state estimation, weighted least squares**

I. Introduction

There is increased penetration of customer-owned low carbon technology devices in modern power networks including DGs like PVs and ESUs. As a result, there is a change in the net demand profiles of customers connected to these networks [1]. The changes in load profiles are often times difficult to predict and also have direct influence on the states of the power network (i.e. node voltages and phase angles). Consequently, the traditional SE based on constant deterministic load model is neither sufficient nor accurate for assessment of operation of modern distribution networks [2]. For instance, with ESUs, it is expected that the load profile will be smoothened, but it is still not very clear to network operators how the networks states will change when both PVs and ESUs are integrated at several customer premises.

Power systems SE is the process of evaluating the voltages and phase angles of the network buses from imperfect measurements at a specific time [3], [4]. SE process has variable measurements which include voltage magnitudes and angles [5]. Interestingly, there have been considerable improvements in the acquisition of these measurements through the use of intelligent electronic devices (IEDs) and phasor measurement units (PMUs) [6].

The first author appreciates the partial funding provided by EFACEC, Porto, Portugal.

Considering the transmission level of the power network, SE is well-known and implemented using several methods. SE on transmission level can be very accurate and is based on high-end perfect data from PMUs; moreover, there are few buses in such systems [3]. However, this is not the case for distribution networks due to the enormous number of buses and it would be impractical to install PMUs at every bus. Other researchers have proposed pseudo-measurement to improve the accuracy of SE [7]. However pseudo-measurements are considered poor quality data because they are based on load forecasting, an estimation of active and reactive power load [8].

Load profile modelling of low voltage networks is not trivial given the random behaviour of load profile at this level of the network. Generally, load profile modelling or load forecasting is influenced by customer factors such as the type of load, period (peak or off-peak), and the weather conditions [3]. Despite the difficulties in modelling traditional customer loads, the increasing penetration of customer-owned low carbon technology devices makes this task more complex.

Historically, power system SE studies and improvements go way back to the era between 1969 and 1989. The WLS technique was discovered by Fred Schweppe and this original form of WLS is still used up-to-date [9]. Further modifications have also been made by researchers for specific studies such as snapshot WLS for transmission level SE [3]. Other techniques such as Kalman filter is widely used in the meshed transmission networks [4]. However, the Kalman filter is considered inefficient for distribution networks due to the lack of true measurements and the poor quality of pseudo-measurements. As a result, WLS has been mostly used in distribution networks regardless of the improvements on Kalman filter techniques [10].

Despite that WLS is the most famous approach in SE, there are other approaches such as the fast decoupled state estimation (FDSE), Hachtels augmented matrix (HAM) and exact second order state estimation (ESOSE). In [11], a detailed comparison between the methods was performed. It was argued that WLS performed better than the others. In [12], [13], WLS method was extended to use probabilistic based model for pseudo-measurements while [8] compared that model with correlation approach and argued that GMM as a statistical model is more accurate.

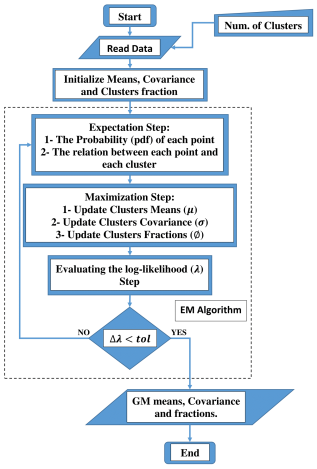


Fig. 1: GMM and EM algorithm flowchart

Although works similar to that presented in this paper have been carried out in [7], [13] for high voltage distribution network, neither of the above published works considered the integration of DGs (PVs and ESUs) and its influence on the customer load profile for modern low voltage networks. This technical work therefore addresses that challenge. The power balance equations for the network have been modified to take into account the net import/export power from the hybrid (PV and energy storage) systems and these have been integrated into the GMM modelling technique. Also, the constraint equations for the PV and energy storage units have been embedded into the state estimation formulation; thus, depicting practical LV network conditions.

This technical work is considered useful for electricity utility operators, distribution system operators (DSOs) and the distribution network operators (DNOs), for the planning, operation and control of their systems

II. Gaussian Mixture Model

The modern load profile has been modelled using GMM. GMM is considered a superposition solution from several Gaussian mixtures/clusters. Fig. 1 flowchart describes the steps of GMM. The probability density function of GMM is (1).

$$GMM_{pdf} = \sum_{i=1}^{I} \pi_i G_{pdf} = \sum_{i=1}^{I} \pi_i G\left(\mu_i, \sigma_i^2\right) \tag{1}$$

Each cluster has a specific mean (μ), variance (σ^2) and weight (π), called the GMM parameters. Expectation-Maximization (EM) algorithm was used to obtain these parameters by solving a log-likelihood optimisation. GMM can be applied to 1-dimension of data or d-dimensions using the relations (2) and (3) [13].

$$G\left(x|\mu,\sigma^2\right) = \frac{1}{\sqrt{2\pi\sigma^2}} \exp\left(-\frac{1}{2\sigma^2}\left(x-\mu\right)^2\right) \tag{2}$$

$$\begin{aligned} G\left(x|\mu,\Xi\right) &= \frac{1}{\left(\sqrt{2\pi}\right)^d \sqrt{\det(\Xi)}} \exp(\Gamma) \\ \Gamma &= \left(-\frac{1}{2}\left(x-\mu\right)^T \Xi^{-1}\left(x-\mu\right)\right) \end{aligned} \tag{3}$$

where x is the data sample and Ξ is the covariance matrix of the multivariate Gaussian distribution.

III. Reduced Gaussian Mixture Model

The reduced GMM is a modified method that aims to increase the accuracy of the GMM pdf approximation by combining some of the mixtures together. However, as [13] argued, this requires updating the weights, means and variances of the new clusters which will be less than the previous number of clusters I i.e. $\sum_{i=1}^{I} \pi_i \neq 1$. The updated values of the cluster parameters are obtained by (4), (5) and (6) [13], where j refers to the mixture to combine, and Co is the covariance matrix.

$$\pi_{i(new)} = \sum \pi_{j(combined)} \tag{4}$$

$$\mu_{i(new)} = \frac{1}{\pi_{i(new)}} \sum_{j}^{I} \pi_j \mu_j \tag{5}$$

$$\begin{aligned} \mathrm{Co}_{i(new)} &= \frac{1}{\pi_{i(new)}} \sum_{j}^{I} \pi_j \left[\mathrm{Co}_j + \xi_j\right] \\ \xi_j &= \left(\mu_j - \mu_{i(new)}\right)\left(\mu_j - \mu_{i(new)}\right)^T \end{aligned} \tag{6}$$

IV. State Estimation

SE can be explained based on the classical equations [3]:

$$z = h(x) + e \tag{7}$$

$$h(x) = \begin{bmatrix} h(x)_1 & h(x)_2 & \dots & h(x)_n \end{bmatrix}^T \tag{8}$$

where, $z = \begin{bmatrix} z_1 & z_2 & \dots & z_n \end{bmatrix}^T$ is the measurements vector with n measurements, x is the state variable vector, $h(x)$ is a vector of nonlinear equations evaluated at the state variable x, e is a zero-mean Gaussian distribution $N(0, R_{ii})$ noise, and R_{ii} is a diagonal matrix that contains all measurements variances, $R_{ii} = \mathrm{diag}\begin{bmatrix} \sigma_1^2 & \sigma_2^2 & \sigma_1^2 & \dots & \sigma_1^n \end{bmatrix}^T$ [14].

The state variable vector for a system of n buses is $x = \begin{bmatrix} \theta_1 & \theta_2 & \dots & \theta_n; V_1 & V_2 & \dots & V_n \end{bmatrix}^T$; the voltage angle of the slack bus (θ_1) is set to zero, and θ_n and V_n are the nth bus voltage angle and magnitude respectively [13]. The WLS algorithm is formulated as an optimisation problem $\min_x F$ aimed to minimise the square of the measurement error e, or residue r.

$$\min_x F = \frac{1}{2}\left(z - h(x)\right)^T R_{ii}^{-1}\left(z - h(x)\right) \tag{9}$$

This problem is reformulated and solved using Newton iterative technique based on the following expressions [13]:

$$\hat{x}_{k+1} = \hat{x}_k + \left[G(\hat{x}_k)\right]^{-1} \nabla F(\hat{x}_k) \tag{10}$$

$$G(x_k) = H^T(x_k) R_{ii}^{-1}(x_k) \tag{11}$$

$$H(x) = \frac{\partial h(x)}{\partial x} \tag{12}$$

$G(x_k)$ is the Gain matrix and $H(x)$ is the Jacobian matrix.

A. Power flow calculation

The nonlinear measurement functions $h(x)$ are expressed as equations related to the current flow between buses, the power flow in the lines and the power injected into a bus [5]. Power injection at bus i (real P_i and reactive Q_i):

$$h_1(x) = P_i = \sum_{j \epsilon N_i} P_{ij} = V_i \sum_{j \epsilon N_i} V_j \left(G_{m_{ij}} \cos(\theta_{ij}) + B_{m_{ij}} \sin(\theta_{ij})\right) \tag{13}$$

$$h_2(x) = Q_i = \sum_{j \epsilon N_i} Q_{ij} = V_i \sum_{j \epsilon N_i} V_j \left(G_{m_{ij}} \sin(\theta_{ij}) - B_{m_{ij}} \cos(\theta_{ij})\right) \tag{14}$$

Power flow from bus i to j (real P_{ij} and reactive Q_{ij}) powers:

$$h_3(x) = P_{ij} = V_i^2 \left(gs_{ij} + g_{i-sh}\right) - V_i V_j \left(gs_{ij} \cos(\theta_{ij}) + bs_{ij} \sin(\theta_{ij})\right) \tag{15}$$

$$h_4(x) = Q_{ij} = -V_i^2 \left(bs_{ij} + b_{i-sh}\right) - V_i V_j \left(gs_{ij} \sin(\theta_{ij}) - bs_{ij} \cos(\theta_{ij})\right) \tag{16}$$

Current flow from bus i to j, I_{ij}:

$$h_5(x) = I_{ij} = \frac{\sqrt{P_{ij}^2 + Q_{ij}^2}}{V_i} \tag{17}$$

If shunt admittance $(g_{i-sh} + jb_{i-sh})$ is ignored, then:

$$h_5(x) = I_{ij} = \sqrt{\left(gs_{ij}^2 + bs_{ij}^2\right)\left(V_i^2 + V_j^2 - 2V_i V_j \cos(\theta_{ij})\right)} \tag{18}$$

where i and j are from and to buses respectively, V_i is voltage magnitude and θ_i is phase angle where $[\theta_{ij}] = \theta_i - \theta_j$, $(G_{m_{ij}} + jB_{m_{ij}})$ is the (i, j) element of the complex admittance matrix, $(gs_{ij} + jbs_{ij})$ is the series admittance, $(g_{i-sh} + jb_{i-sh})$ is the shunt admittance, N_i is the count of the set of buses connected to bus i [5]. The customer's load profile (LP) after integrating PVs and ESUs is realised from (19):

$$P_{New(LP)} = P_{LP} - P_{PV} \pm P_{ESU} \tag{19}$$

where if $P_{New(LP)} > 0$, then power is imported from the grid; otherwise, if $P_{New(LP)} < 0$, then the customer is exporting power to the network. The expressions in (13) and (14) were modified by the introduction of (19) and thus modifying the GMM parameters. The flowchart in Fig. 2 describes the WLS implementation procedure.

B. WLS State Estimation and GMM

In SE, the GMM of customer load profile was considered in the modelling of WLS pseudo measurements. Given that the load data were acquired through measurements, it was considered in this study that the impacts of time of day and weather variations have been accounted for already. The load at a given node was considered to be independent of the load at the other nodes. The procedure for obtaining the GMM

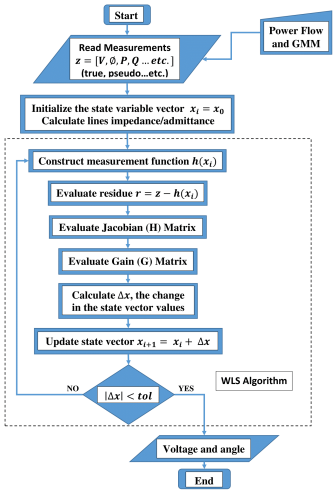


Fig. 2: WLS algorithm flowchart

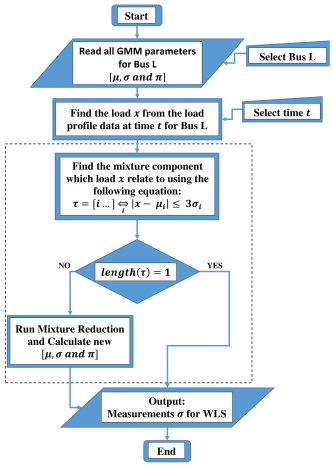


Fig. 3: GMM measurements for WLS flowchart

parameters required for the WLS algorithm is illustrated in Fig. 3 flowchart. In some cases, the observed load is connected to more than one mixture component $(\text{length}(\tau) > 1)$, leading to two or more measurement variances for the same load x. In this case, reduced GMM was applied to ensure that the load x is connected to a single variance [7], [13].

V. ESU MODEL: CHARGING AND DISCHARGING

The ESUs data were represented with simulated data. A Simulink model was built to simulate a lithium-ion Shepherds battery charging and discharging processes [15], with PV (Fig. 4) or grid only (Fig. 5). PVD is PV data while LPD is Load Profile Data. The discharging and charging of energy is controlled by the equations (20) and (21) respectively [15]:

$$V_T(it, i^*, i) = V_0 - \frac{K.Q.(i + i^*)}{(Q - it)} - \frac{K.Q.it}{(Q - it)} + A \exp\left(-B.it\right) \tag{20}$$

$$V_T(it, i^*, i) = V_0 - \frac{K.Q.(i + i^*)}{it + (0.1Q)} - \frac{K.Q.it}{(Q - it)} + A \exp\left(-B.it\right) \tag{21}$$

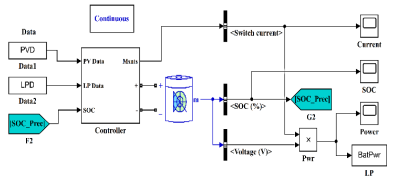


Fig. 4: Simulink model for ESUs charged from PVs

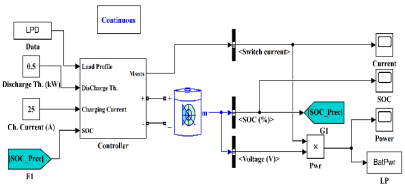


Fig. 5: Simulink model for ESUs charged from the Grid

where V_T is battery terminal voltage, V_0 is constant voltage, K is polarization constant in V/Ah, i^* is low frequency current dynamics in A, i is battery current, $'it'$ is extracted capacity in Ah, Q is maximum battery capacity in Ah, A is exponential voltage. B is exponential capacity in Ah^{-1} [15]. The controller block acts as a simple converter and charger model, it controls the direction of the current (in/out), the maximum charging current, and the load threshold to start charging from the grid.

VI. Case Study

GMM was used to model one-day load profile of 55 customers with a 1-minute resolution and this was programmed in MATLAB. Data for the 50Hz low voltage European test feeder was obtained from [16]. The network was considered to be relatively balanced. The PV data was obtained from UK Power Networks (UKPN) data store for 20 substations and 10 domestic houses [17]. A part of that PV data was used in this study, that is, data of selected days in summer of 2014. The ESUs data were simulated using Simulink battery model. openDSS [18] was used to run the power flow calculations and to obtain the true measurements of the WLS state estimator. The software was combined with MATLAB.

A. Network description

The low voltage radial distribution map diagram for the test European feeder is shown in Fig. 6. This network is located in Kent, England [19]. The network comprised 905 buses, 55 household customers and the distribution substation. The network frequency is 50 Hz; a 3-phase $\triangle/Y$-grounded transformer at the substation steps down the voltage from 11kV to 0.416kV. The substation was considered a voltage source with 11kV (1.05 p.u) sending-end voltage in the simulation. For the sake of simplicity, several customer loads were lumped, thereby reducing the number of load nodes in the modified network. This modification of the test system is reasonable given the relatively balanced nature of the network. The test system is as shown in Fig. 7. The low voltage network performance was evaluated under different load profile scenarios.

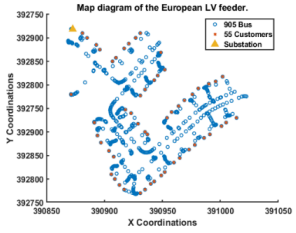


Fig. 6: Map diagram of the European LV feeder.

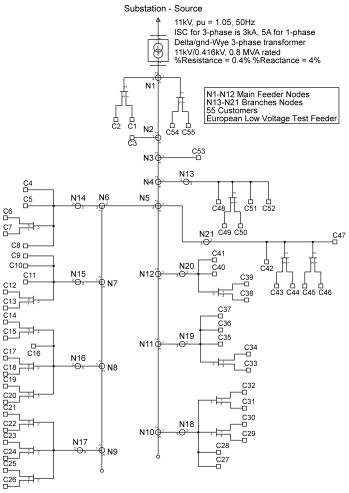


Fig. 7: One-line diagram of the LV network.

These scenarios include load profiles without PVs or ESUs, with PVs alone, ESUs only and combined PVs and ESUs. The study assumed that PV and ESUs were DC-coupled in the customers household.

B. Battery (ESU) characteristics

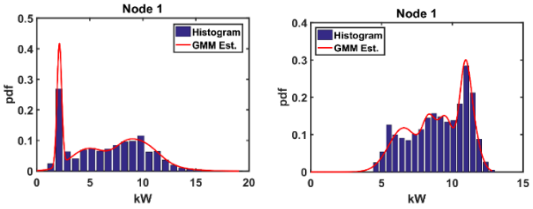
TABLE I: Battery details

Parameter	Definition
V_0	Nominal Voltage 24 VDC
V_{full}	Full Charged Voltage 30 VDC
V_{cutoff}	Cut-off Voltage 18.4 VDC
K	Polarization Constant 0.0039 V/Ah
Q	Battery Capacity 100 Ah
A	Exponential Voltage 4.07 V
B	Exponential Capacity 0.4684 Ah^{-1}
R	Internal Resistance approx. 2mΩ at 25 deg. C

The battery was modelled using Shepherds model and the datasheet of 24V/100A battery of Clayton Power [20]. The parameters were calculated according to [15], and the main characteristics are shown in Table I.

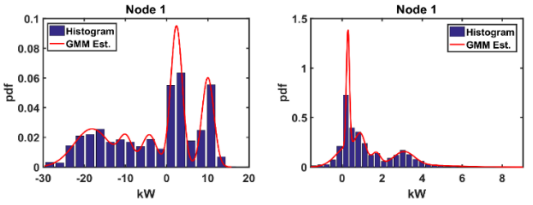
C. Load Profile Modelling Using GMM

The figures (Figs. 8 - 9) below show the probability density at node 1 for different network scenarios. The bars represent the histogram probability density of the aggregated load profile. The red line represents the GMM probability density function with 5 clusters.



(a) Without PV/ESU (b) With ESU

Fig. 8: GMM pdf



(a) With PV (b) With PV and ESU

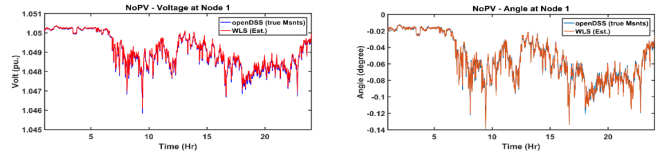
Fig. 9: GMM pdf

D. State estimation of test network

Figs. 10 - 13 show the voltage magnitudes and some phase angle plots for node 1 (N1). We have shown plots for node 1 as the goal of the research is to provide enhanced information to the network operator about their system performance for different levels of proliferation of their network with customer-owned PV and ESUs. There is also space constraint and so all result plots could not be shown. As seen from the network diagram, N1 is the secondary side of the utility transformer.

In the first scenario, the network was assumed to have no PV or ESU. Voltage drop occurred especially during peak hours, after 07:00 and after 16:00 (see Fig. 10). The maximum voltage drop occurred at minute 566 (09:26) and reached 1.0458 p.u while the WLS estimated voltage drop at the same time was 1.0461 pu - an error of 0.0003 pu.

Integrating PV alone caused a voltage rise issue due to customers exporting excess PV power generation to the grid. From Fig. 11, during the period 09:00 and 16:00 the voltage rise is between 1.052 and 1.058 pu. The Scottish Power Group estimated the voltage tolerance to be between 0.987 pu and 1.1 pu. In this case therefore, the voltage rise is still not a big issue that may require PV power curtailment or reactive power control. However, due to the absence of PV power in



(a) Voltage magnitude (b) Voltage angle

Fig. 10: Estimated voltage magnitude and angle when no DG integration

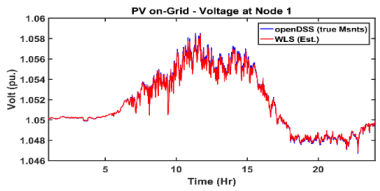
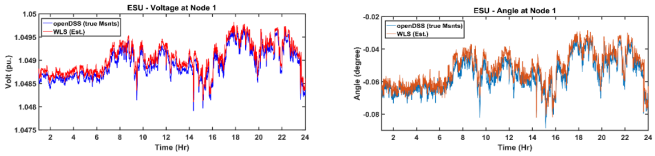


Fig. 11: Voltage magnitude: network with PV on-grid



(a) Voltage magnitude (b) Voltage angle

Fig. 12: Estimated voltage magnitude and angle: network with ESUs.

the evening, voltage drop may still appear (max. 1.047 pu).

In the third scenario, the network was assumed to have ESUs installed in customers households with 30% state of charge (SOC). It is shown in Fig. 12 that the network faced voltage drop during the night after 23:00 and until 7:00 in the morning. This was due to batteries been charged from the grid at this time. However, as soon as the batteries were fully charged, the voltage improved. Moreover, the maximum voltage drop reached was 1.0484 pu during the charging period and this was still better than the first scenario where voltage dropped to 1.0458 pu. There were no high voltage drops during the afternoon and the evening, since the batteries covered the load demand during these periods. This scenario is called demand shifting, and the voltage drop settled between two levels: 1.0486 and 1.0498 pu. Retrofitting the rooftop PVs with

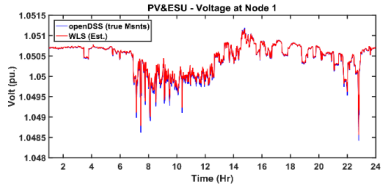


Fig. 13: Voltage magnitude for network with PV and ESUs

the ESUs in customers households reduced the power exported to the grid. This was because the excess power generated was used to charge the batteries. Thus, the maximum voltage rise was reduced from 1.058 pu to 1.0511 pu (Fig. 13) which is safer for the grid. Moreover, Fig. 16 shows that the ESUs were able to secure the network from large voltage drops.

E. State estimation accuracy

The Tables II and III contain the average absolute error (AAE) and the root mean square error (RMSE) between the true values from openDSS and the estimated values from WLS for voltage magnitude. WLS SE errors are small for the voltages in all cases as shown in the tables. This high

TABLE II: SE error: voltage

	Without PV/ESU	With ESU
AAE(%)	0.005747	0.012203
RMSE (pu)	0.000073	0.000130

TABLE III: SE error: voltage

	With PV on-grid	With PV and ESU
AAE (%)	0.007739	0.002265
RMSE (pu)	0.000111	0.000036

accuracy in the estimation is expected since the node is close to the substation (Node 1). The errors are calculated as in (21) and (22), where N is the data length, $\hat{r}$ is the estimated value and r is the true value.

$$\text{AAE} = \frac{100}{N}\sum|\frac{(\hat{r}-r)}{r}| \tag{22}$$

$$\text{RMSE} = \sqrt{\frac{1}{N}\sum(\hat{r}-r)^2} \tag{23}$$

In Table II (with ESU), the error values are higher than the values in other scenarios. This was due to GMM and the calculation of measurement variances. In this case, GMM was unable to allocate some of the loads in the 3σ range, because the variance values were small with large clusters number. To address this, the number of clusters was reduced to 3.

VII. Conclusion

This paper has presented the implementation of GMM and WLS SE for an LV distribution network with significant penetration of PVs and ESUs. Firstly, the GMM method was used to separate customers load profiles into several load groups. Each group was represented by a GM pdf. The EM approach was used to determine GMM components parameters. These parameters were used for the WLS state estimation algorithm to improve its results. Secondly, the SE of the network was implemented using WLS technique.

The true measurements needed for the WLS implementation were obtained from load flow calculations using the openDSS software. Pseudo measurements and variances (uncertainty) were obtained from GMM. The SE was carried out for four different scenarios of the network: without PV/ESU, PV, ESU, and with PV and ESU. The summary is:

- The network without DGs experienced voltage drop during peak hours (in the morning and evening).
- Integrating PV alone resulted in voltage rise around midday due to excess PV power generation been exported to the grid. Such case revealed the need for PV power curtailment or ESUs installation to avoid voltage exceeding the standard limits.
- Integrating ESUs alone acted as a demand shifter, the demand was shifted away from high load periods to low load periods.
- Integrating PV and ESU reduced the voltage drop during peak hours. However, voltage rise occurred when the ESUs were fully charged and PV generation was still higher than the demand.

In addition, relatively small errors were noticed between the results of the WLS estimated values and the true measurements.

References

[1] P. Grahn, V. Briggner, L. Johansson, D. Babazadeh, L. Nordstrom, and D. Babazadeh,"Centralized versus distributed state estimation for hybrid AC/HVDC grid," in 2017 IEEE PES Innovative Smart Grid Technologies Conference Europe (ISGT-Europe), 2017, pp. 1-6.

[2] S. Paudyal, C. A. Canizares, and K. Bhattacharya, "Optimal Operation of Distribution Feeders in Smart Grids," IEEE Transactions on Industrial Electronics, vol. 58, no. 10, pp. 4495-4503, Oct. 2011.

[3] A. Monticelli, State Estimation in Electric Power Systems: A Generalized Approach. Springer Science & Business Media, 1999

[4] C. Carquex, C. Rosenberg, and K. Bhattacharya, "State Estimation in Power Distribution Systems Based on Ensemble Kalman Filtering," IEEE Transactions on Power Systems, vol. 33, no. 6, pp. 6600-6610, Nov. 2018.

[5] A. Abur and A. Gomez-Exposito, Power System State Estimation: Theory and Implementation. CRC Press, 2004.

[6] M. Ingram, S. Bell, S. Mathews, G. J. Cokkinides, and A. P. Meliopoulos, "Use of Phasor Measurements, SCADA and IED Data to Improve State Estimation Procedures," In Proceedings of the 2004 Georgia Tech Fault and Disturbance Analysis Conference, Atlanta, Georgia, April, pp. 26-27, 2004.

[7] R. Singh, B. C. Pal, and R. A. Jabr., "Distribution system state estimation through Gaussian mixture model of the load as pseudo-measurement," IET Gener. Transm. Distrib., vol. 4, Iss. 1, pp. 50 59, Jan. 2010.

[8] A. K. Singh, S. K. Ibraheem, and M. Muazzam, "An Overview of Electricity Demand Forecasting Techniques," National Conference on Emerging Trends in Electrical, Instrumentation & Communication Engineering, vol. 3, 2013.

[9] M. B. D. C. Filho, A. M. L. Silva, and D. M. Falcao, "Bibliography on power system state estimation (1968-1989)," IEEE Transactions on Power Systems, vol. 5, no. 3, pp. 950-961, 1990.

[10] S. Huang, C. Lu, and Y. Lo, "Evaluation of AMI and SCADA Data Synergy for Distribution Feeder Modeling," IEEE Transactions on Smart Grid, vol. 6, no. 4, pp. 1639-1647, 2015.

[11] A. Sengupta and A. K. Sinha, "A comparative study on state estimation algorithms," in 2007 International Conference on Industrial and Information Systems, 2007, pp. 317-322

[12] A. K. Ghosh, D. L. Lubkeman, M. J. Downey, and R. H. Jones, "Distribution circuit state estimation using a probabilistic approach," IEEE Transactions on Power Systems, vol. 12, no. 1, pp. 45-51, 1997.

[13] R. Singh, B. C. Pal, and R. A. Jabr, "Statistical Representation of Distribution System Loads Using Gaussian Mixture Model," IEEE Transactions on Power Systems, vol. 25, no. 1, pp. 29-37, 2010.

[14] E. Manitsas , R. Singh, B. Pal, and G. Strbac, "Modelling of pseudo-measurements for distribution system state estimation," in CIRED Seminar 2008: SmartGrids for Distribution, 2008, pp. 1-4.

[15] E. Raszmann, K. Baker, Y. Shi, and D. Christensen, "Modeling stationary lithium-ion batteries for optimization and predictive control," 2017 IEEE Power and Energy Conference at Illinois (PECI), pp. 1-7, 2017.

[16] European Low Voltage Test Feeder [Online]. Available: https://ewh.ieee.org/soc/pes/dsacom/testfeeders/

[17] Photovoltaic (PV) Solar Panel Energy Generation data [Online]. Available: https://data.london.gov.uk/dataset/photovoltaic–pv–solar-panel-energy-generation-data

[18] OpenDSS - EPRI Distribution System Simulator [Online]. Available: https://sourceforge.net/projects/electricdss/files/OpenDSS/

[19] A. Navarro and L. N. Ochoa, "Dissemination Document "Low Voltage Networks Models and Low Carbon Technology Profile"," ed: The University of Manchester, 2015.

[20] Lithium Ion Batteries [Online]. Available: http://www.claytonpower.com/products/lithium-ion-batteries